



Spring-dashpot vibrational model for the investigation of viscoelasticity in gelatinous abrasive media and subsequent control of parameters for the blast polishing of Ti-6Al-4 V alloy

Quintin de Jongh¹ · Ramesh Kuppuswamy^{1,2} · Matthew Titus¹

Received: 18 March 2022 / Accepted: 27 July 2022

© The Author(s), under exclusive licence to Springer-Verlag London Ltd., part of Springer Nature 2022

Abstract

Blast polishing offers an operator-friendly solution to many of the previously encountered polishing difficulties. However, the process lacks studies into the control of key parameters, one of which is viscoelasticity (particularly present in biological-based abrasive medias). Together with analytical-empirical models, a vibrational spring-dashpot model is presented, which characterizes the impact force, contact time, and damping ratio/coefficient of polishing media upon impact; as well as the effects of damping on contact parameters: stress, deformation, and area of contact. These are compared to experimentally gathered results for verification of the model. Impact force is shown to decrease dramatically with increasing hydration while increasing linearly with an increase in kinetic energy. Experimental findings reveal that 50% wet contact exhibits a 340% reduction in force magnitude compared to dry contact. Contact time results show an exponential increase with an increase in hydration. Research findings also show that higher hydration levels result in lower damping ratios and that higher kinetic energies (related to higher hydration levels) tend toward a decrease in damping ratio. Similarly, media damping coefficients decrease with both hydronal increases and kinetic energy increases. Results show that contact stress is reduced at higher hydration levels, which is mainly due to higher contact areas, and hence it was noticed that an increase in hydration prevents occurrence of chipping and brittle failure on the workpiece surface. Contact stress is shown to reduce by 325% from a 10% wet contact to a 50% wet contact. A high hydration of 30 to 50%, a high impinging velocity of value 31.4 m/s and above, a low stand-off distance of value 20 mm and below, a 45° polishing angle, and a polishing time of 20 to 40 min provide the most optimal parameters for efficient polishing to achieve a mirror finish on an additive manufactured Ti-6Al-4V component. The findings stipulated provide a base on which to further characterize the process and aim to promote further development and optimization of the blast polishing process.

Keywords Blast polishing · Vibrational modeling · Viscoelastic · Spring-damper · Contact mechanics

Abbreviations

MAP	Magnetic abrasive polishing
SLS	Standard linear solid
AFM	Atomic force microscopy
SLM	Selective laser melted
TMD	Tuned mass damper
AM	Additive manufactured
MQL	Minimum quantity lubrication

1 Introduction

Advanced manufacturing is highly applicable in industry where tolerances are becoming smaller and materials more difficult to manufacture. Finishing processes, such as polishing, are critical to providing desired material properties, finishes, lessening corrosion, and to extending service life. This is applicable to many modern industries (aero-space, biomedical, and advanced automotive). Creating a controllable process is censorious to efficiency and optimization in industry, allowing for the inherent saving of resources and time. Blast polishing (also known as Aerolap polishing [1]) is a mechanical finishing manufacturing process that allows for the achievement of a fine surface roughness of value less than 0.1 µm [2]. Other polishing techniques including magnetic abrasive polishing (MAP), laser polishing and

✉ Quintin de Jongh
djinqui001@myuct.ac.za

¹ University of Cape Town, South Africa, Cape town, South Africa

² Atria Institute of Technology, Bangalore, India

electropolishing, involve either a large amount of operator experience, high process cost, and high abrasive media costs, are limited in shape/material compatibility, and/or the process parameters are difficult to control [1, 3, 4]. The blast polishing process offers a solution to these encountered problems by reducing the required operator experience and background knowledge to a minimum, as well as by reducing process costs and increasing material/shape compatibility. The blast polishing action occurs by means of ductile failure, where asperity peaks fold into the valleys, causing flattening and subsequent smoothening [5]. Analytical models based on the notion of momentum require that the time of contact be broadly estimated, while empirical models require many experimental results and may not produce accurate results under conditions outside of the experimental range. Many developed models ignore the important factor of abrasive viscoelasticity upon impact. A vibrational model, using a spring-dashpot system (Kelvin-Voigt type model), has been developed and is presented, to aid in the understanding of abrasive media viscoelasticity, which varies as a function of the water content of the media. Also, a previously developed force model [6] has been modified and extended to allow for the estimation of forces at varying hydration levels and elastic moduli. The outputs of the model presented in this manuscript are expected to support further AM development, particularly on process optimization, through provision of several controllable process parameters. This will have direct implications and benefits for the manufacturing and advanced manufacturing industries, as the process will become more viable to industry and easier to implement. Experiments regarding forces in blast polishing are lacking and models of viscoelasticity for the blast polishing process have not been presented before, thus the results presented here are of importance to the study of both the polishing process and as well as the Ti-6Al-4V material.

2 Past research

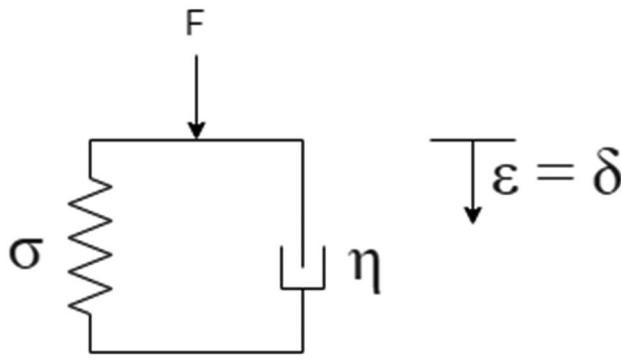
Several damper models have been developed in attempts to improve manufacturing process design. Wang et al. [7] optimized the chatter control of a cutting tool by using a mass damper model (a Euler–Bernoulli beam model). Naghieh et al. [8] developed a viscoelastic contact model for elastomers and polymeric coatings. Finite element models have been used extensively to model viscoelastic impact problems. A notable solution is provided by Assie et al. [9], who produced a low-velocity (< 30 m/s) model for the analysis of a viscoelastic structure contact. The authors used a Wiechart model to simulate the internal damping occurring within the structure [9]. This is because the Wiechart model describes both creep and relaxation adequately. The problem is converted into a

static problem by use of the Newmark method and the Lagrange multiplier technique is used to incorporate the contact condition [9]. Their solution involved three phases with multiple steps each. The preprocessor phase involves the input of the following data: material data, time increment and steps, suitable element, mesh generation, initial conditions, boundary conditions, total contact nodes, contact constraints, and input history [9]. The processor phase is more complex and involves generating matrices for stiffness, mass, damping, and load vector, before applying constraints and solving for the required output [9]. The postprocessor phase involves repetition and storing material history [9]. Solutions were acquired for one-, two-, and three-dimensional problems (for force and displacement) and these lined up well with classical viscoelastic models used by other researchers [10, 11]. FEM, however, is not the only technique used to model viscoelastic contacts and other techniques have also been implemented by researchers in the field. Lopez-Guerra and Solares [12] executed multiple approaches to atomic force microscopy (AFM) simulation through varying from a simple linear spring dashpot system to a nonlinear system capable of accurately reproducing viscoelastic surface properties. The response was once again analyzed in terms of force–displacement curves as well as dissipated energy. By analyzing the various spring-dashpot models, the authors were able to highlight strengths and deficiencies that occurred while in contact with the AFM tip. Fukumoto et al. [13] presented extensive research on the blast polishing process. In their report, they displayed a large set of results regarding the influence of water content in polishing media and how it affects the process. The authors were polishing tungsten carbide surfaces and used polishing hydration levels of 10%, 30%, and 50%, impacting at velocities of 55.8 m/s, 48.7 m/s, and 41 m/s, respectively. They used a high-speed camera (250,000 frames/s) to measure the impact time of various hydrated media and found that contact time increased significantly from a wetness of 10% (approximately 10 μ s) to a wetness of 50% (approximately 70 μ s) [13]. They thus found that measured impact forces decreased significantly from 2 to 0.5 N for 10% hydration and 30% hydration respectively.

Another method of spring-damper modeling is that of the Kelvin-Voigt's (see Fig. 1), as the instantaneous contact only exhibits creep and not stress relaxation.

The Kelvin-Voigt model is characterized by (1), where strain is equivalent in the damper and the spring, but the total stress is the sum of the stress experienced in the spring and the stress experienced in the damper [14].

$$\sigma(t) = E\varepsilon(t) + \eta \frac{d\varepsilon(t)}{dt} \quad (1)$$

**Fig. 1** Kelvin-Voigt viscoelasticity model**Fig. 2** Image of blast polishing machine, developed at the advanced manufacturing lab (UCT)

This is then solved to:

$$\epsilon(t) = \frac{\sigma_0}{E} \left(1 - e^{-t/\tau_R} \right) \quad (2)$$

where:

$$\tau_R = \frac{\eta}{E} \quad (3)$$

σ is the stress experienced, t is the time, ϵ is the strain experienced, σ_0 is the initial stress, η is the viscosity of the damper, and τ_R is the retardation time [14]. Proper calculation of contact time is of utmost importance when developing a force control model or attempting to describe process parameters such as contact stress and deformation. Using the principle of momentum conservation is a popular method to calculate contact time [1]. Past research by Roberts et al. [15] shows the measurement of contact time in short duration sports ball impacts. A golf ball is assumed hit by a titanium golf head and this makes the study particularly relevant to this proposed model. Hocknell [16] showed that a reasonable estimated of impact duration (contact time) could be made using the following formula derived from Hertz Law (adapted by Goldsmith [17]):

$$\tau = 4.53 \left[\frac{m_B(\delta_A + \delta_B)}{\sqrt{R_B v_{imp}}} \right]^{\frac{2}{5}} \quad (4)$$

where:

$$\delta_A = \frac{1 - v_A^2}{\pi E_A} \quad (5)$$

$$\delta_B = \frac{1 - v_B^2}{\pi E_B} \quad (6)$$

The subscript B denotes the abrasive and A denotes the workpiece.

m is the abrasive mass, R is the radius of abrasive, v_{imp} is the impinging velocity, v is the Poisson's ratio of each respective material, and E is the elastic modulus of each respective material.

Past research has shown that multiple methods of process modeling exist and that important results have been gathered for the polishing process. Results gathered by Fukumoto et al. [13] are of notable interest to this study and show that increased hydration (and thus viscoelasticity) decreases impact force substantially while higher impinging velocities result in greater rates of material removal. Conclusively, the past research analyzed has provided a basis on which to further process optimization, design experiments, and aid the creation of polishing models.

3 Experimental set up

To carry out blast polishing experiments that allowed the authors to acquire comparable and verifiable results to the presented and created vibrational model, a blast polishing machine was designed and developed. The machine uses compressed air to recycle gelatinous media (approximately 2 mm in diameter) coated in #5000 diamond powder and #3000 SiC powder and subsequently blasts this out of an impeller system at output velocities varying between 6.28 and 31.4 m/s. The media travels a stand-off distance of 20 mm to impart ductile regime polishing conditions to a workpiece.

The media is then collected in a bin and continually hydrated using an MQL before being recycled back to the impeller. Figures 2 and 3 show the developed machine used to carry out experiments.

The measured polishing outputs and their measurement methods were:

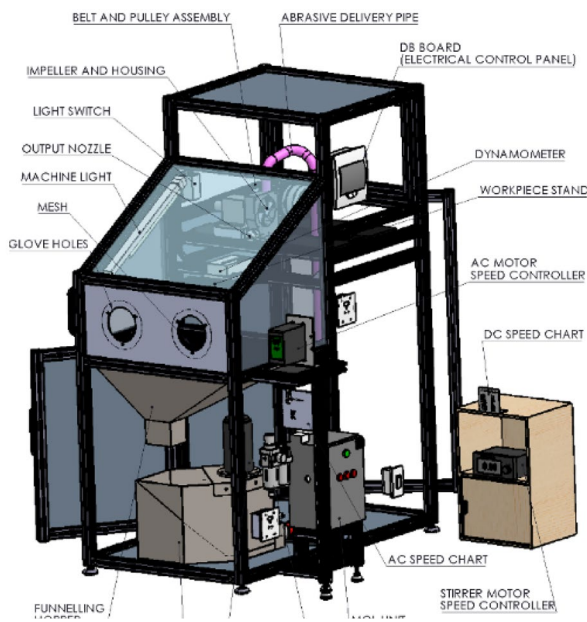


Fig. 3 Labeled blast polishing machine diagram

- Surface roughness parameters: R_a , $R_{y_{max}}$, and R_z , using a Taylor Hobson Surtronic 3P Profilometer.
- Surface texture, topography, and quality measurements (qualitative), using an FEI Nova NanoSEM and MIRA Tescan 3.
- Live signal analysis for force (using a Kistler 9625 dynamometer), images (FLIR C5 thermal video camera), and vibrational measurements (using a Kistler 8772A50 accelerometer). Figure 4 shows the experimental set-up

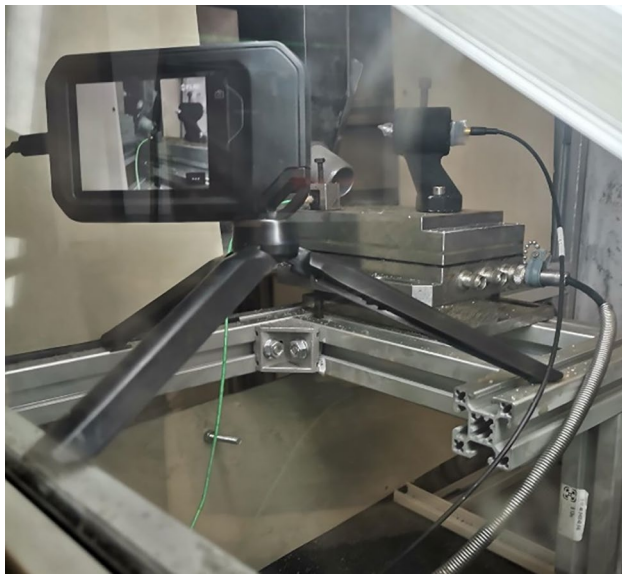


Fig. 4 Experimental set-up with video

including dynamometer, accelerometer, imaging camera, and microphone.

Process parameters are important to understand when designing experiments and when creating models. Media shape and size is important in that the choice of it can affect surface markings and material removal rate (spherical, deformable abrasives are the best) [18], while impinging angle should be allowed for a balance between horizontal and vertical force components [19]. Polishing time needs to be long enough to achieve the required surface roughness while not slowing down efficiency and impinging velocity should be high enough to allow for optimal MRR [1, 6, 19]. Media should be wettable and hydration levels should allow for the control of viscoelasticity (which means a lower convergence value of surface roughness and more preferential markings) [20]. Stand-off distance should be low to minimize impinging velocity loss and change of angle while nozzle output area should be small enough to allow for a directed output to the workpiece [1, 6, 21]. Some polishing parameters can be changed during process runs, e.g., impinging velocity while other must be set permanently, e.g., nozzle output area.

3.1 Design of experiments and workpiece/media preparation

To gather relevant, accurate, and reliable results, a thorough DOE was performed. SLM produced Ti-6Al-4 V cubes with initial R_a values of $6 \mu\text{m} \pm 2 \mu\text{m}$ were acquired and then surface ground to $0.8 \mu\text{m} \pm 0.15 \mu\text{m}$. The cubes were then cleaned in an ultrasonic cleaner to remove impurities and stored in a soft silk cloth until polishing occurred. Cubes

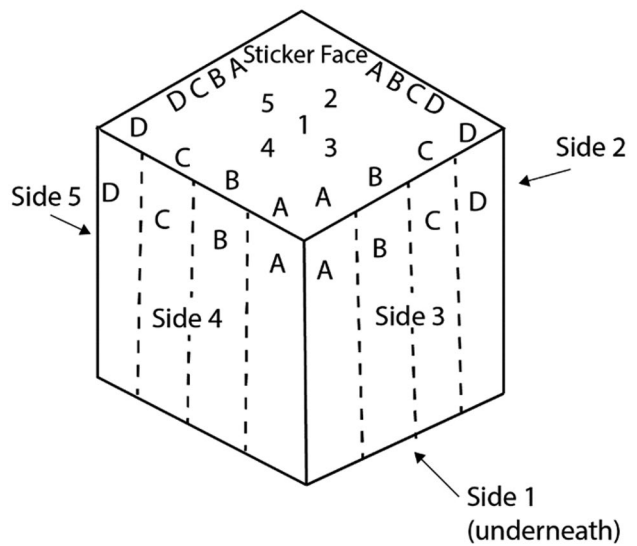


Fig. 5 Workpiece in custom stand before polishing

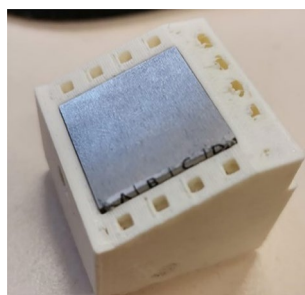


Fig. 6 Workpiece divisions for experiments

were polished at different conditions, notably with a change in hydration and/or a change in impinging velocity. Hydration steps were 10%, 30%, and 50% while velocity steps were 6.28 m/s, 15 m/s, and 31.4 m/s.

The cube faces were split into numerous subdivisions to run multiple experiments on each face (for each time division), see Figs. 5 and 6.

Each individual face was designated an experiment at a specific hydration or velocity interval, see Table 1 for an example of how experiments were set up for one sample.

Table 2 describes the parameters (both varying and constant) at which experiments were run. The varying parameters are notably polishing time, media hydration levels, media impinging velocity, and media diamond concentration.

The abrasive media properties used in the experiment are as in Table 3 [6]:

Figure 7 shows a microscopic image ($32 \times$ magnification) of the gelatin core used and shows diameter measurements across the length of the cores. Multiple images were gathered for various hydration levels, and it was found that media increased by approximately 0.5 mm from the dry condition to the 50% wet condition. Note that gelatin was chosen due to its capacity to absorb water easily and due to its ability to be easily coated. Other research using bio-cores [2, 6, 13] also use gelatin as the media core.

Table 2 Parameters at which experiments were run

Parameters (details)	Units	Lower limit to upper limit
Impinging velocity	m/s	6.28–31.4
Standoff distance	mm	20
Polishing time	Seconds	30–2700
Abrasive water content	%	10–50
Workpiece inclination angle	°	45
Diamond mesh size	#	5000
Diamond concentration	%	0.1–0.5

4 Analytical modeling

The model described below shows the derivation of meaningful contact results (stress, force, damping ratio, contact time) through a vibrational spring-dashpot model.

4.1 Force model and material properties

To make an adequate comparison of hydration results, kinetic energy is matched over hydration levels and is increased based on the dry impinging velocities. Mass increases as hydration is increased and thus the velocity of impact is lessened as hydration is increased (thereby keeping a constant kinetic energy).

The dry abrasive mass is found by assuming a spherical abrasive, knowing the radius of the abrasive, and knowing the density of the abrasive. This gives an overall mass of 0.35605 mg (at a radius of 0.5 mm).

At dry impact, the impinging velocities vary and are taken at the following intervals: 6.28 m/s, 15 m/s, 31.4 m/s, 45 m/s, and 60 m/s. These correspond to kinetic energies of 0.07 mJ, 0.040 mJ, 0.175 mJ, 0.3605 mJ, and 0.6409 mJ respectively.

Velocities (m/s) for increasing hydration levels are then found to be as follows (see Table 4):

Abrasive properties used in this model are as stipulated in Table 3. Workpiece properties used are 113 GPa for the elastic modulus of Ti-6Al-4 V and 0.342 for the Poisson's ratio of Ti-6Al-4V [6].

Table 1 Example of experimental conditions for one sample

Experiment number and conditions	Division number → Side number ↓	A	B	C	D
AS1: 31.4 m/s, 10% hydration, 0.1% diamond	1	2.5 min	10 min	25 min	45 min
AS2: 15 m/s, 10% hydration, 0.1% diamond	2	2.5 min	10 min	25 min	45 min
AS3, 6.28 m/s, 10% hydration, 0.1% diamond	3	2.5 min	10 min	25 min	45 min
BS1, 31.4 m/s, 30% hydration, 0.1% diamond	4	2.5 min	10 min	25 min	45 min
BS2, 15 m/s, 30% hydration, 0.1% diamond	5	2.5 min	10 min	25 min	45 min

Table 3 Material properties of abrasive constituents

	Gelatin	SiC	Diamond	Water
Constituency (%)	47, 67, 87, or 97	2.9	0.1	0, 10, 30, or 50
Density	680	3020	3500	997
Diameter	1 mm	2.5 μm	2.5 μm	N/A
Elastic modulus	43.2 kPa	330 GPa	1100 GPa	N/A
Poisson's ratio	0.680	0.3020	0.3500	0.5

Variation in elastic modulus and density while increasing hydration is the last important derivation of material property. Note that elastic modulus is a measure of object/material stiffness. Fukumoto et al. [13] measured its change (the static modulus of abrasive) as wetness was increased. For a wetness of 0%, 10%, 30%, and 50%, they found elastic modulus to be 43.2 kPa, 7.8 kPa, 0.78 kPa, and 0.52 kPa respectively. Using the law of mixtures, the elastic modulus of the abrasive is determined by:

$$E_{abr} = \left(\frac{\%_{water}}{E_{water}} + \frac{\%_{gelatin}}{E_{gelatin}} + \frac{\%_{SiC}}{E_{SiC}} + \frac{\%_{diamond}}{E_{diamond}} \right)^{-1} \quad (7)$$

Using the determined elastic modulus from Fukumoto et al. [13], it was found that water has a contributing elastic modulus of 0.9 kPa. This led to the following output (Fig. 8):

After material property analysis, a model for force was developed. Adaptations and modifications were made to a previously developed model [6] (by the authors) to ascertain the contact forces for various hydration levels (at multiple kinetic energies). The model is based on sets of developed and verified empirical formulae as well as hertzian contact mechanics.

Derivations based on the notion of critical values (the point at which a material changes behavior from elastic to plastic) were made, and the output of impinging force at a particular kinetic energy (and relative impinging velocity) was determined to be:

$$F_{imp} = F_c \left(\frac{\omega(V)}{\omega_c} \right)^{3/2} \quad (8)$$

While F_{imp} can also be calculated by the widely used (by substituting $w(V)$ into the equation) [22]:

$$F_{imp} = \frac{4}{3} E' \sqrt{R} [w(V)]^{3/2} \quad (9)$$

where:

$$F_c = \frac{4}{3} \left(\frac{R}{E'} \right)^2 \left(\frac{C}{2} \pi S_y \right)^3 \quad (10)$$

$$\omega_c = \left(\frac{\pi C S_y}{2 E'} \right)^2 R \quad (11)$$

$$\omega(V) = \left(\frac{5V^2 m_{abr} \omega_c^{3/2}}{4F_c} \right)^{2/5} \quad (12)$$

E' is the combined elastic modulus of the workpiece and abrasive:

$$\frac{2}{E'} = \frac{1 - v_1^2}{E_1} + \frac{1 - v_2^2}{E_2} \quad (13)$$

v_1 and v_2 are the workpiece and abrasive Poisson's ratios respectively and E_1 and E_2 are the workpiece and abrasive elastic moduli respectively. R is the radius of the abrasive

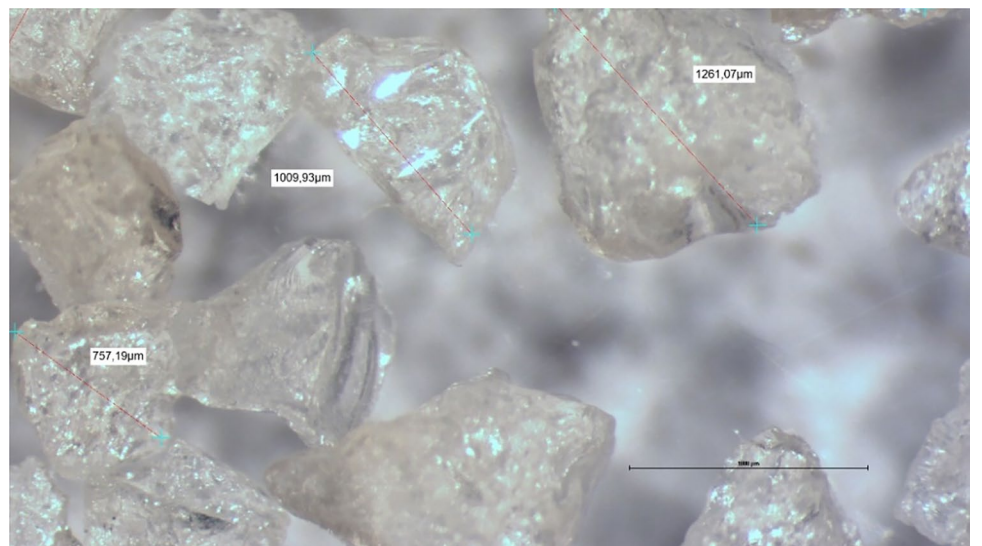
Fig. 7 Gelatin microscopic image

Table 4 Impinging velocities at various hydration levels for constant kinetic energies across hydration levels

10% Hydration				
5.9877	14.3019	29.9387	42.9058	57.2078
30% Hydration				
5.2516	12.5436	26.2580	37.6309	50.1745
50% Hydration				
4.8890	11.6775	24.4449	35.0325	46.7099

(combined abrasive is not applicable if the assumption of sphere interacting with a plane is true). C is the critical yield stress coefficient:

$$C = 1.295e^{0.736V} \quad (14)$$

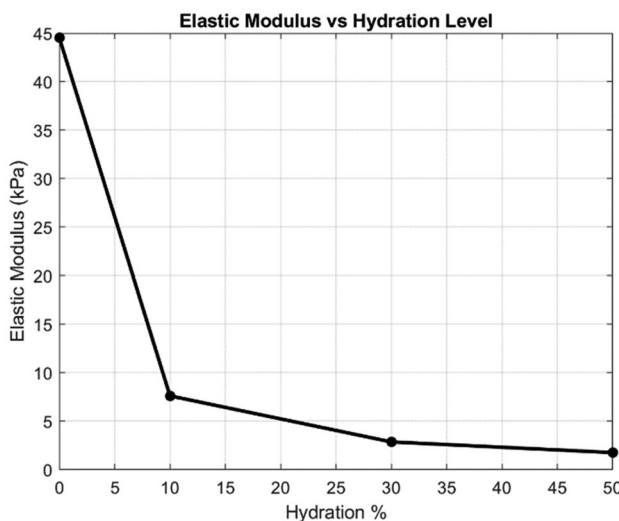
S_y is the yield strength of the abrasive (210 kPa [6]). V is the impinging velocity of the abrasive upon the workpiece. m_{abr} is the abrasive particle's mass. Note that critical velocity is given by:

$$V_c = \sqrt{\frac{4\omega_c F_c}{5m_{abr}}} \quad (15)$$

The ratio of impinging velocity to critical velocity is important as it ensures that the use of the developed model is applicable. If V/V_c is greater than 1, the equations cannot be used as the collision would incur plastic deformation. For all values of hydration and maximum impinging velocities, the ratio is less than 1 and therefore these equations are applicable.

Contact is estimated by:

$$A = A_C \omega(V) \quad (16)$$

**Fig. 8** Elastic modulus of abrasive as a variation of hydration level**Table 5** Abrasive properties at various hydration levels

$m_0 = 0.356mg$	$\rho_0 = 680 \text{ kg/m}^3$	$R_0 = 0.500 \text{ mm}$	$E_0 = 43.2 \text{ kPa}$
$m_{10} = 0.392mg$	$\rho_{10} = 702 \text{ kg/m}^3$	$R_{10} = 0.512 \text{ mm}$	$E_{10} = 7.61 \text{ kPa}$
$m_{30} = 0.509mg$	$\rho_{30} = 752 \text{ kg/m}^3$	$R_{30} = 0.545 \text{ mm}$	$E_{30} = 2.87 \text{ kPa}$
$m_{50} = 0.5875mg$	$\rho_{50} = 809 \text{ kg/m}^3$	$R_{50} = 0.558 \text{ mm}$	$E_{50} = 1.765 \text{ kPa}$

Which allows for the estimation of contact stress by the typical contact stress equation for a plane interacting with a sphere:

$$\sigma = \frac{1.5F_c}{A} \quad (17)$$

Contact area is also assumed as circular and thus contact area equals:

$$A = \pi a^2 \quad (18)$$

where a is the radius of circular contact, and from contact mechanics, the area of contact can be expressed in terms of deformation:

$$A = \pi(2\delta R - \delta^2) \quad (19)$$

Knowing the abrasive size and density, the volume and associated mass for different water contents is calculated (as water content is a direct function of abrasive mass):

$$V_{abr} = \frac{4}{3}\pi R_{abr}^3 \quad (20)$$

$$m_{abr} = (1 + H\%) \rho_{abr} V_{abr} \quad (21)$$

It is important to note that with varying hydrations, the mass, radius, density, and elastic modulus of the combined abrasive change as follows (see Table 5):

Change in radius can be calculated by assuming the abrasive is spherical in nature and then deriving the radius from the mass:

$$r = \sqrt[3]{\frac{3m}{4\rho\pi}} \quad (22)$$

Elastic modulus and density vary as mentioned previously.

It was found that force decreases with a sharp initial decrease as hydration level is increased, while force increases with a gentle initial increase as kinetic energy is increased. See Fig. 9 for a visual representation. The values of force and trend of sharp-initial increase to gentle-final increase show agreement with the measured experimental forces stated in Table 6 as well as by those stipulated by Fukumoto et al. [13] and Kuppuswamy et al. [1].

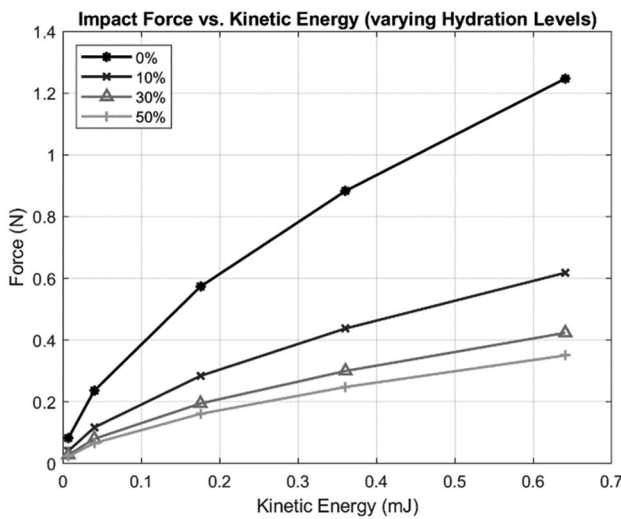


Fig. 9 Impact force as a function of kinetic energy (for various hydration levels)

Calculations for contact time could then be completed (in order to establish the damped frequency of contact for the vibrational model). These were acquired by dividing the product of the respective velocity (at a particular kinetic energy) and abrasive mass by the impinging force of the abrasive:

$$t_{contact} = \frac{m_1 v_1}{F_{imp}} \quad (23)$$

Contact time shows a sharp initial decay as kinetic energy is increased (tending towards a limit as energy increases). Contact time increases greatly as hydration is increased (with a large step occurring between 10 and 30%) (see Fig. 10). The results stipulated by Fukumoto et al. [13] (who used a high speed camera to determine contact time) are incredibly similar to the results achieved in this model (with dry contact exhibiting around 20 μ s contact time and 50% wet contact exhibiting between 80 and 100 μ s contact time). Kuppuswamy et al. [1] used a similar model to determine contact time.

4.2 Spring dashpot model

In addition to the multi-layered nature of the multi-con abrasive (gelatin-SiC-diamond), an incredible variety of effects

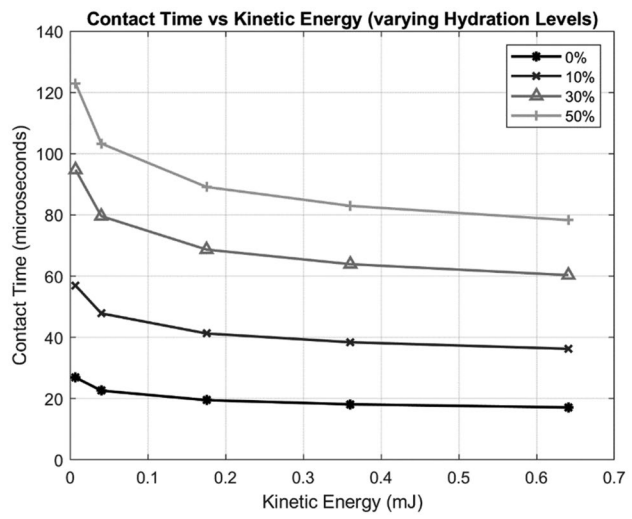


Fig. 10 Contact time as a function of kinetic energy (for varying hydration levels)

can be achieved with minimal changes to the process design by manipulating abrasive parameters. The model described in the following sub-chapters characterizes the effect of hydrating the abrasive media to different levels, firstly to prove that the addition of moisture aids in reducing contact stress and thus enables ductile regime polishing conditions to occur at higher than usual velocities, and secondly, to create a series of relations and inputs for further research to occur (namely that of defined damping ratios and damping coefficients).

4.2.1 Basis of model and assumptions

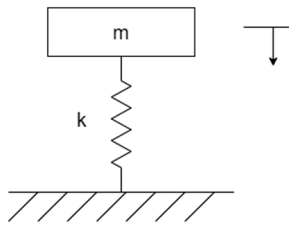
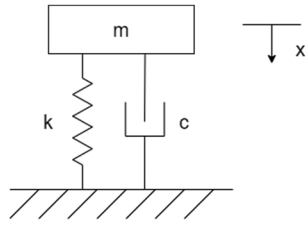
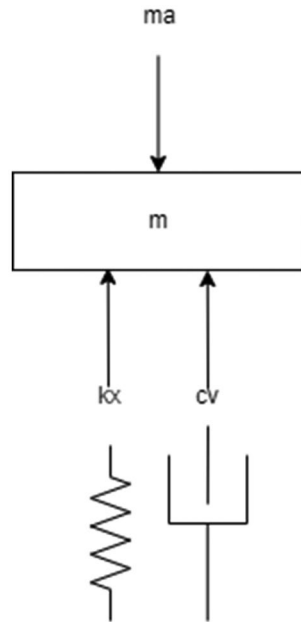
Figures 11 and 12 show the models used at further analysis, where m represents the mass of the abrasive, c represents the damping due to hydration (a desired output of this research), k represents the combined stiffness of the abrasive system, and x represents the deformation of the abrasive. The fixed ground is assumed as the workpiece of the material (which in this case would be a flat AM produced Ti-6Al-4V component). As per the Kelvin-Voigt model, an undamped free vibration is chosen as the basis of this model as it incorporates the necessary system parameters (creep), while lessening complications in process design.

Figure 11 shows the first vibrational model used in this research (where the abrasive is assumed to not be hydrated). This allows for a slightly simpler solution which can then be modified to include hydration factors. A key for the models can be seen in Fig. 13.

Using the basis of Hooke's law, the estimation/assumption that spring stiffness is equal to the elastic modulus of the abrasive is made:

Table 6 Experimentally measured forces

Velocity hydration	6.28 m/s	15 m/s	31.4 m/s
10%	1.822 N	2.463 N	3.744 N
30%	1.597 N	1.990 N	3.318 N
50%	1.467 N	1.650 N	2.757 N

**Fig. 11** Spring model for dry contact**Fig. 12** Spring-dashpot model for wet contact**Fig. 14** Force balance on spring dashpot model

$$k_{abr} = E_{abr} \quad (24)$$

An investigation to the force balance (see Fig. 14) is as follows:

$$m\ddot{x} + c\dot{x} + kx = 0 \quad (25)$$

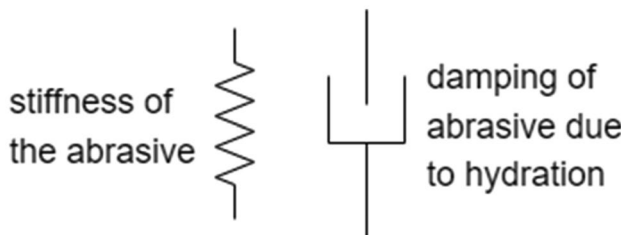
Simplified to:

$$\ddot{x} + 2\zeta\omega_n\dot{x} + \omega_n^2x = 0 \quad (26)$$

where:

$$\omega_n = \sqrt{\frac{k}{m}} = \sqrt{\frac{E}{m}} \quad (27)$$

Noting that the elastic modulus and abrasive combined mass change as hydration changes, the natural frequency will change accordingly. Note that the damping ratio is given by the following equation:

**Fig. 13** Figures key

$$\zeta = \frac{c}{2m\omega_n} \quad (28)$$

where all variables are as stated previously (except t, which is time).

Damped frequency is described by (see Fig. 15):

$$\omega_d = \omega_n \sqrt{1 - \zeta^2} \quad (29)$$

ω_d can be described as the period of contact (where displacement is 0 as contact begins, building up to the largest displacement X before the abrasive begins to return to its original shape and leave the workpiece). See Fig. 15 for a visual description.

The damped frequency can thus simply be described as:

$$\omega_d = \frac{\pi}{t_{contact}} \quad (30)$$

where contact time is used as per (23).

Mass increases with hydration level as stated previously. This means that the natural frequency changes slightly (decreases) as hydration is increased. This implies that the damping coefficient (zeta) will change with varying hydrations. From previously, the contact times for each wetness and velocity increment are known. The contact period and frequency ratio for each hydration level can thus be determined.

Once the damped frequency and natural frequencies are solved for, the damping ratio (ζ) can be found by rearranging (29) to:

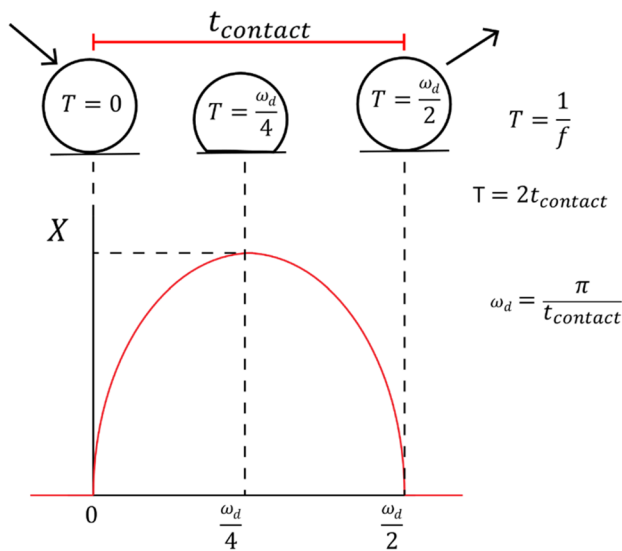


Fig. 15 Description of damped contact frequency

$$\zeta = \sqrt{1 - \left(\frac{\omega_d}{\omega_n}\right)^2} \quad (31)$$

While damping coefficient can be found by rearranging (28):

$$c = 2m\omega_n\zeta \quad (32)$$

After force balance, displacement solutions can be acquired by using vibrational analysis, which leads to the following equation:

$$x(t) = A_1 \sin(\omega_d t) e^{-\zeta \omega_n t} + A_2 \cos(\omega_d t) e^{-\zeta \omega_n t} \quad (33)$$

where: $x(t)$ is the displacement ($\delta(t)$). $A_2 = 0$ because the initial displacement is $x=0$.

While:

$$A_1 = \frac{\dot{x}_o}{\omega_d} \quad (34)$$

x is a measure of the deformation δ and thus as previously stated contact stress can be found by:

$$\sigma = \frac{1.5F_c}{\pi(2\delta R - \delta^2)} \quad (35)$$

4.2.2 Undamped (dry) contact displacement

When damping is not present, damping frequency is not present and the only present frequency is that of natural frequency, leaving the displacement solution as:

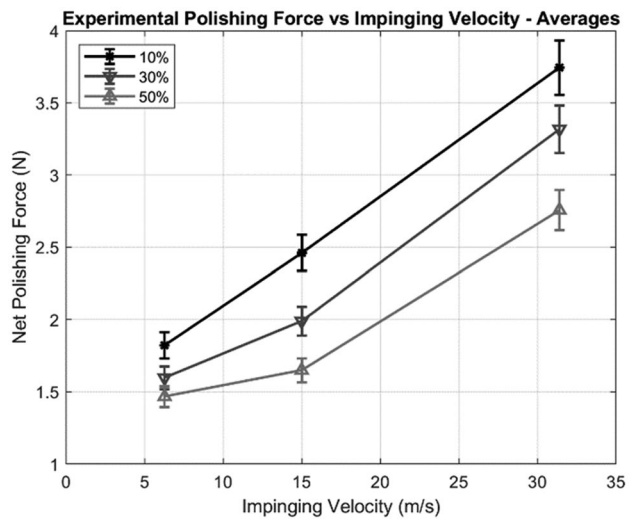


Fig. 16 Experimentally measured impact forces

$$x = \frac{\dot{x}_o}{\omega_n} \sin(\omega_n t) \quad (36)$$

The contact times for an undamped abrasive can be found at various kinetic energies by using the times stated in Sect. 3. The maximum displacement at various kinetic energies can be found ($\sin 90^\circ = 1$, therefore the sin term for maximum displacement can be omitted). Contact stress can be found from (35).

4.2.3 Damped (wet) contact displacement

Displacements (and subsequently the contact areas and contact stresses) for varying hydration levels must be found.

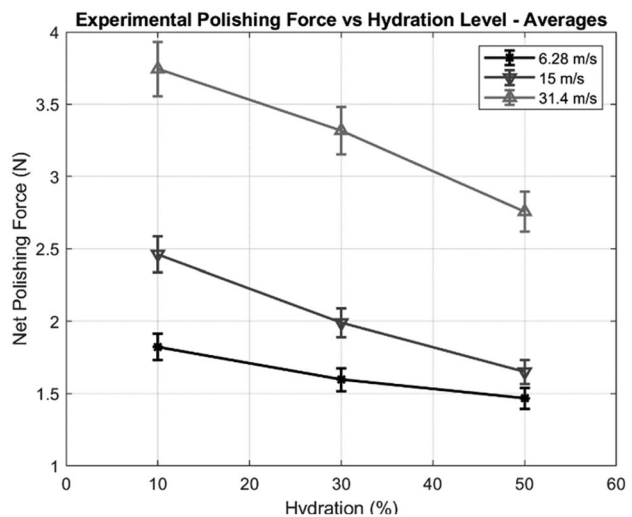


Fig. 17 Experimentally measured impact forces in terms of hydration

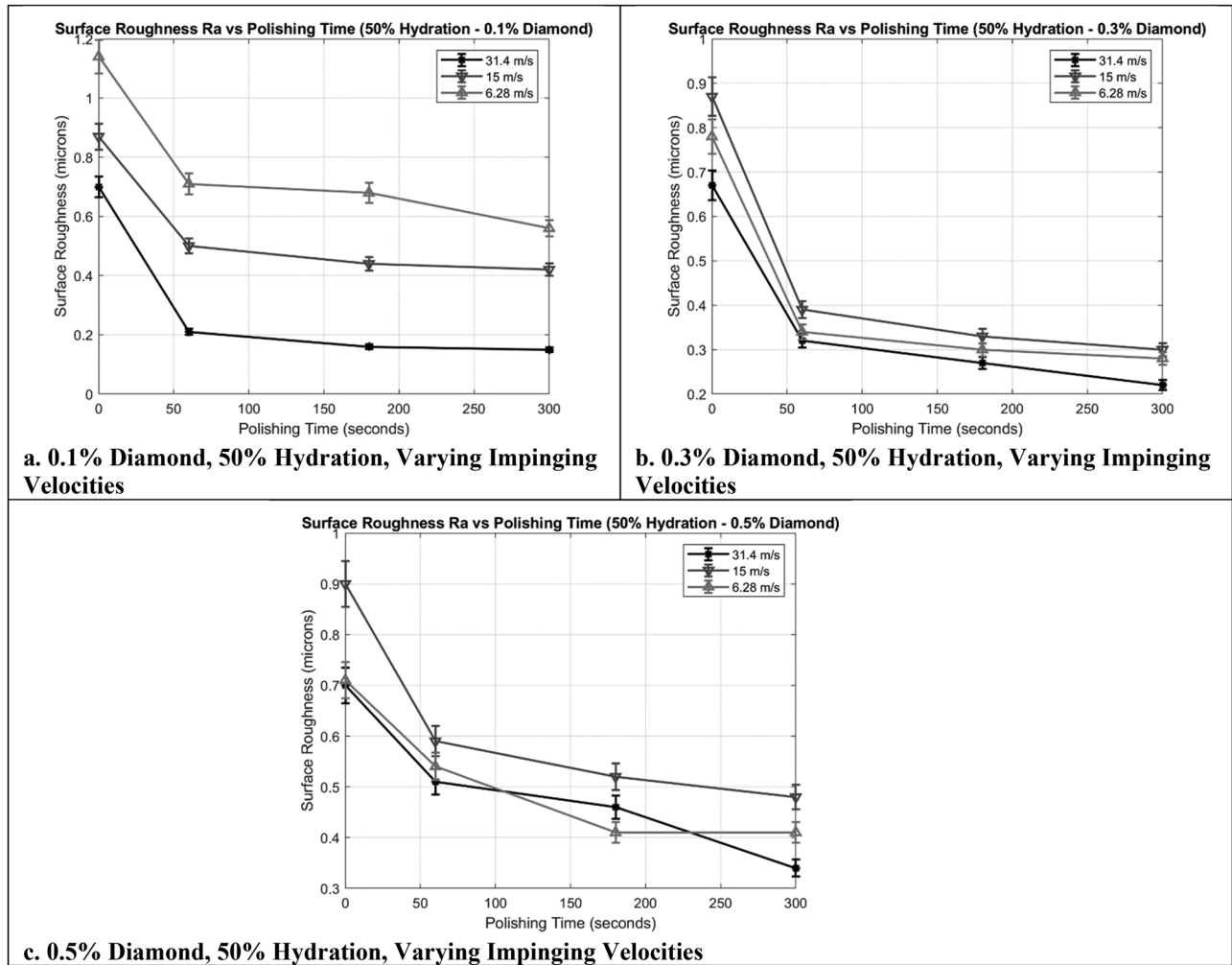


Fig. 18 Surface roughness changes for varying velocities over time (50% hydration). **a** 0.1% diamond, 50% hydration, varying impinging velocities. **b** 0.3% diamond, 50% hydration, varying impinging velocities. **c** 0.5% diamond, 50% hydration, varying impinging velocities

This is slightly more complex in nature than the undamped solution.

The vibrational analysis was continued by first finding coefficient A_1 for each hydration level and associated kinetic energy. The maximum displacements for each case can then be found. Displacements are found by (33).

Finally, the contact stresses for each level of hydration along with its associated kinetic energies are found.

for impact force (an average of 3 experiments for each condition):

This is visually represented in Fig. 17. Figure 16 shows the same results in terms of hydration instead of velocity. Using multivariate linear regression, the following empirical equation for force as a function of both hydration and impinging velocity was acquired:

$$F_{imp} = 1.6876 - 0.01796H\% + 0.066759V_{imp} \quad (37)$$

with an R square value of 0.7580 and a multiple R value of 0.8707.

The values of determined force and the variance in these force results agree with past experimental research results [2, 13] as well as theoretical momentum and empirical models [1, 6] and with the force model stipulated in Fig. 9. These gathered results and the referenced results are used throughout the development of the model to provide verification and validation of the model results.

5 Results and discussion

5.1 Experimental results

5.1.1 Force results

Using the experimental setup and conditions described, the following measurements shown in Table 6 were made

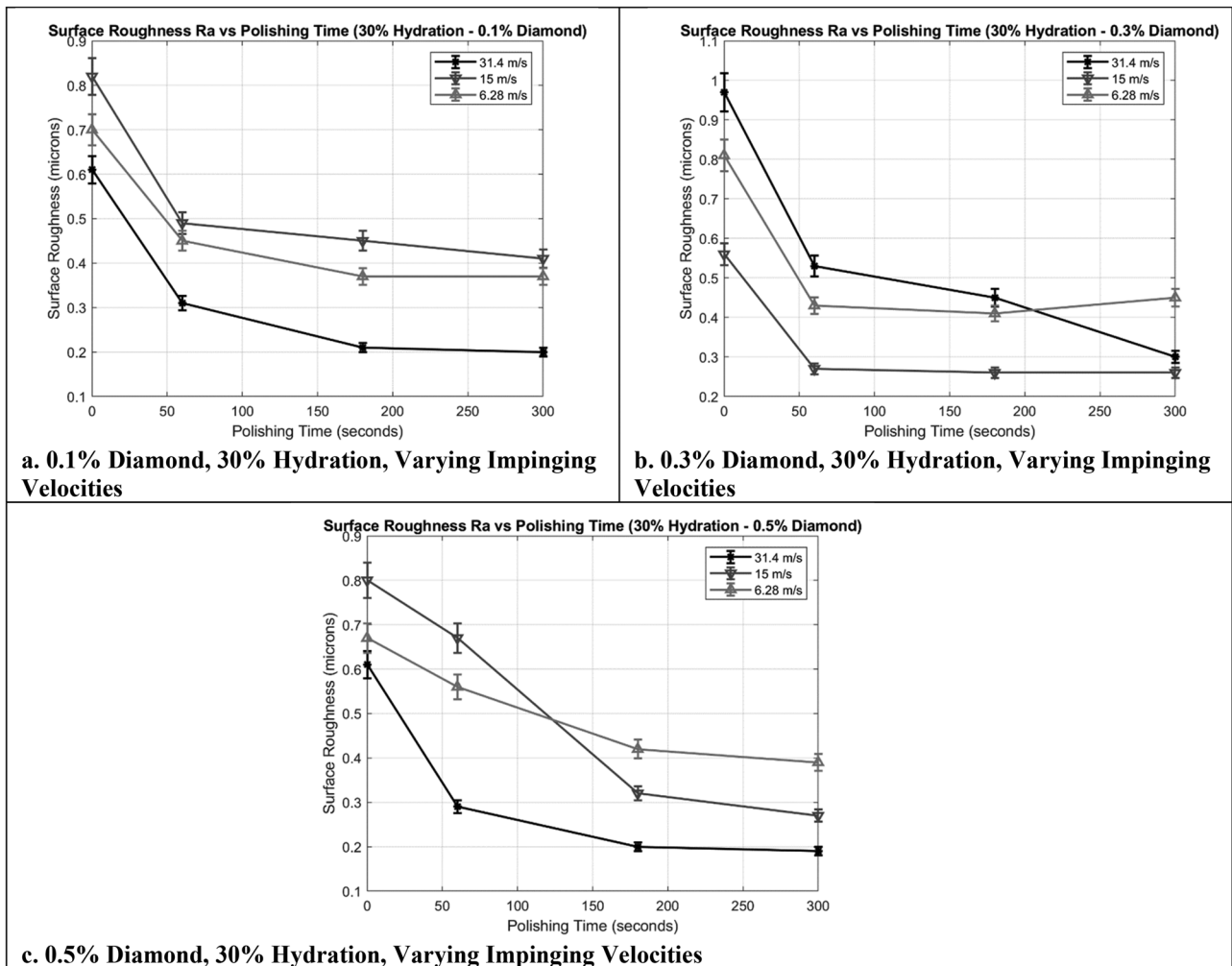


Fig. 19 Surface roughness changes for varying velocities over time (30% hydration). **a** 0.1% diamond, 30% hydration, varying impinging velocities. **b** 0.3% diamond, 30% hydration, varying impinging velocities. **c** 0.5% diamond, 30% hydration, varying impinging velocities

5.1.2 Surface finish/surface texture results

This section is dedicated to displaying surface parameter results acquired from experimentation at various polishing conditions. The below results were acquired over multiple iterations using the developed equipment stated previously. Much of the displayed results are focussed on hydralional changes so that proper comparisons can be made to the vibrational model.

Figure 18 and its inclusive graphs show the effect of polishing at high hydration (50%) over a short period of time while comparing different impinging velocities. The initial sharp decline in surface roughness is entirely apparent over all conditions while higher impinging velocities tend toward a lower convergence surface roughness value. Over a longer period or if a higher kinetic energy was provided, lower surface roughness could certainly be achieved.

The results shown in Fig. 18 agree entirely with those in Fig. 19 (results for a lower hydration level of 30%), aiding in the verification of achieved results that higher impinging velocities aid in a lower level of surface roughness.

Figure 20 does not show a direct relationship between hydration and surface roughness for low values of impinging velocity while for higher values of impinging velocity, the effect of hydration (causing lower surface roughness values) is entirely noticeable. These results agree with researchers [2, 13, 21] who state the higher hydrated media generally have a lower convergence value than lower hydrated media but have a steadier decline rate to achieve these values (i.e., convergence values take longer to reach). Lower kinetic energies/impinging velocities also require longer times to reach convergence, i.e., higher hydrated media at lower polishing times and lower impinging velocities should generally show similar

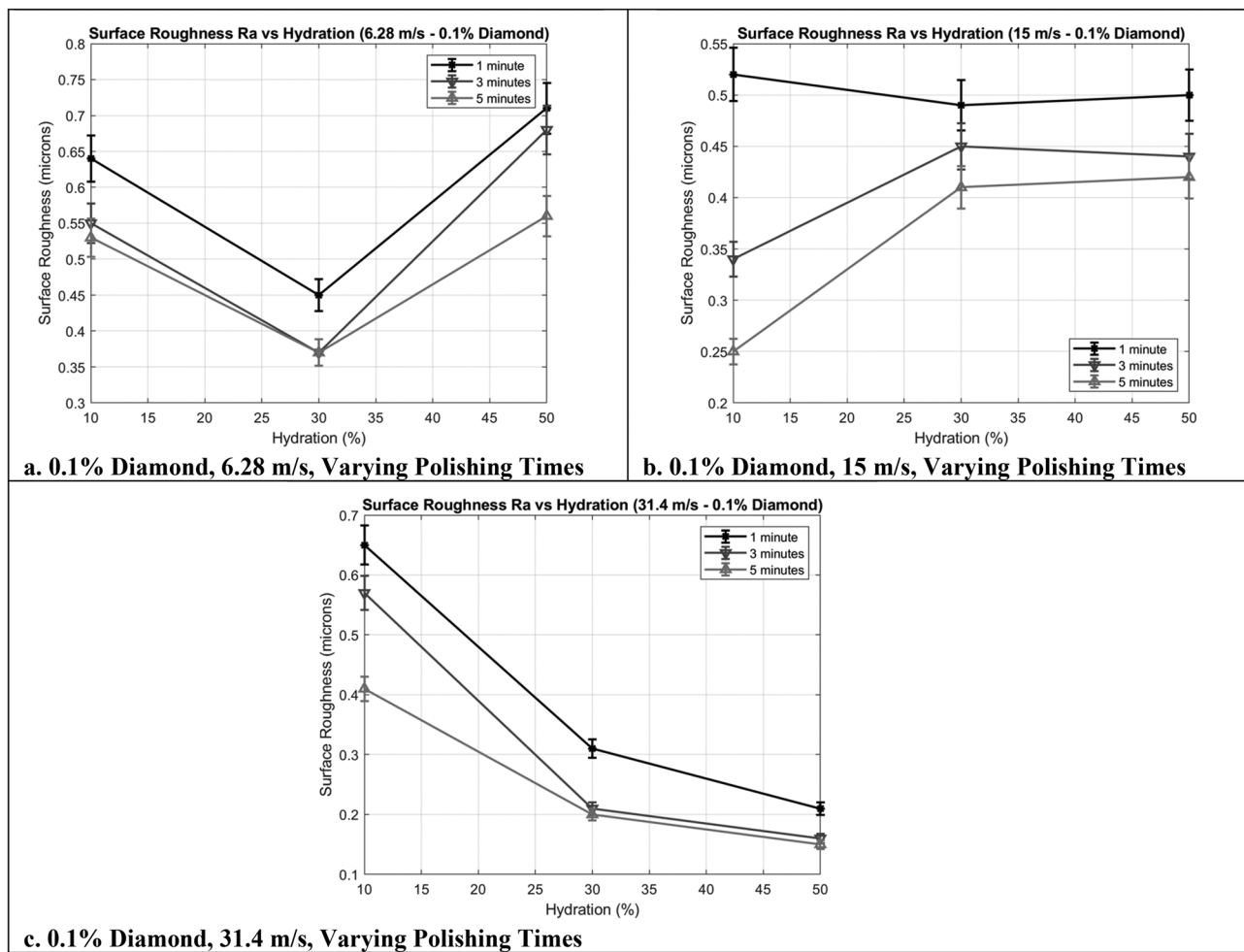


Fig. 20 Surface roughness changes for varying polishing times over hydration (0.1% diamond). **a** 0.1% diamond, 6.28 m/s, varying polishing times. **b** 0.1% diamond, 15 m/s, varying polishing times. **c** 0.1% diamond, 31.4 m/s, varying polishing times

or lower values of surface roughness, which is what is observed above.

Figure 21 aids in proving (as expected) that higher impinging velocities (even over short time periods at high hydration) will lead to lower values of surface roughness (higher rates of material removal).

Figure 22 (at a high magnification of 1500 X) shows the change in surface over 45 min for a low hydration and high impinging velocity. A clear improvement is noted with surface inclusions, pores, and imperfections decreasing significantly while a flatter form becomes apparent too. However, at this low hydration, a presence of minute scratch marks becomes apparent over time.

The two sets of results in Figs. 23 and 24 show the vast improvement in surface quality over time for low polishing time and impinging velocity at a higher hydration (30%). This aids in proving that higher hydration requires minimal time to improve quality (while longer times are required to improve overall roughness).

The results shown in Figs. 25 and 26 (at the same conditions but different magnifications) again aid in proving that hydration plays an important role in the betterment of surface texture and quality. The 50% hydration image shows a flatter overall form, a lesser presence of impurities and scratch marks, and a smoother texture.

5.2 Vibrational model results (theoretical)

The three main results of this analysis (damping ratio, damping coefficient, and contact stress) are shown and discussed in this section, with a focus on how outputs affect the blast polishing process and what they mean to future designs.

The first output of this model is that of damping ratio. Figure 27 below shows that the damping ratio at low kinetic energies is close to critical ($\zeta = 1$) and shows the trend of logarithmic decrease as kinetic energy is increased (becoming more underdamped). Lower damping ratios imply longer stabilization times as well as more oscillations before

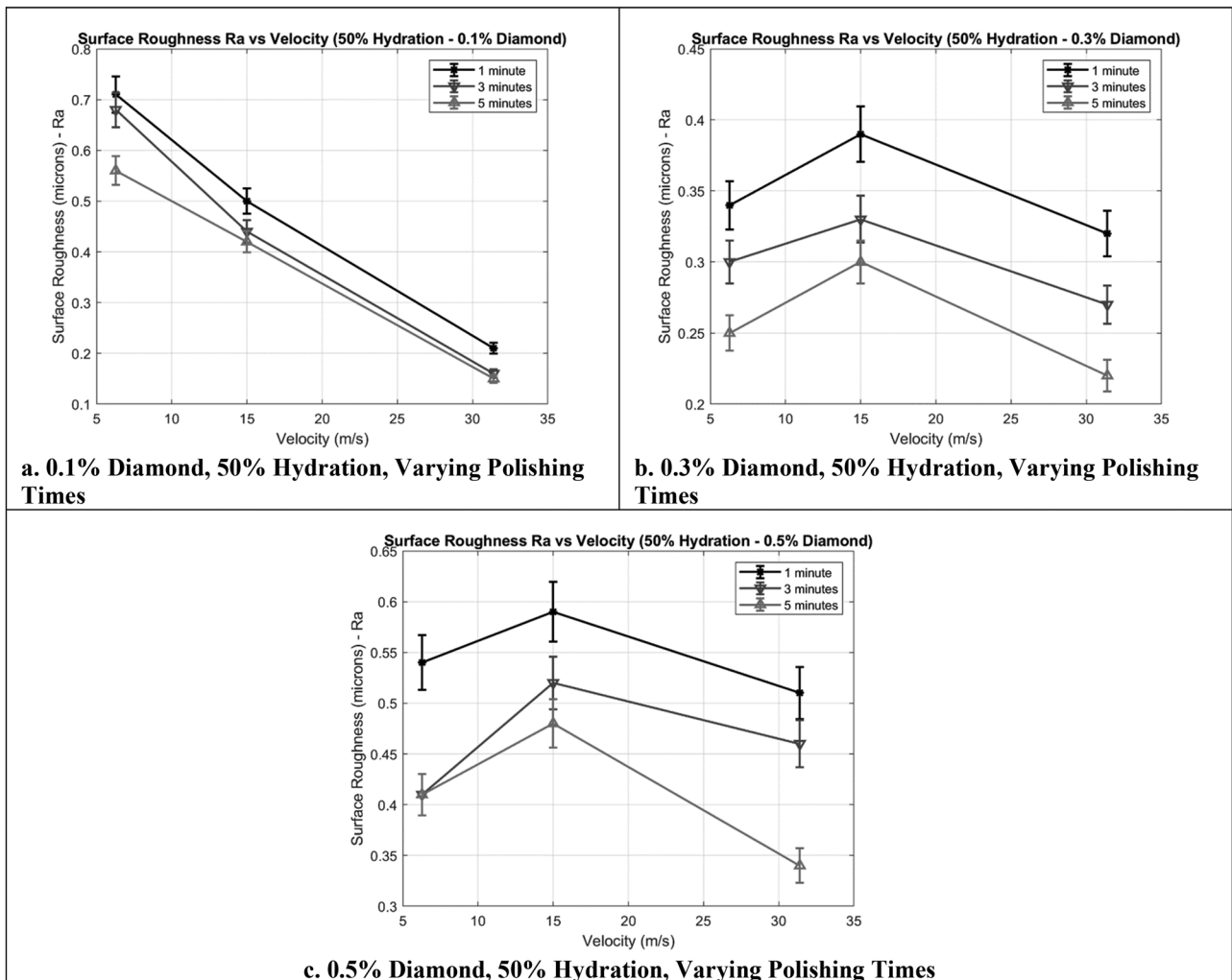


Fig. 21 Surface roughness changes for varying polishing times over velocity (50% hydration). **a** 0.1% diamond, 50% hydration, varying polishing times. **b** 0.3% diamond, 50% hydration, varying polishing times. **c** 0.5% diamond, 50% hydration, varying polishing times

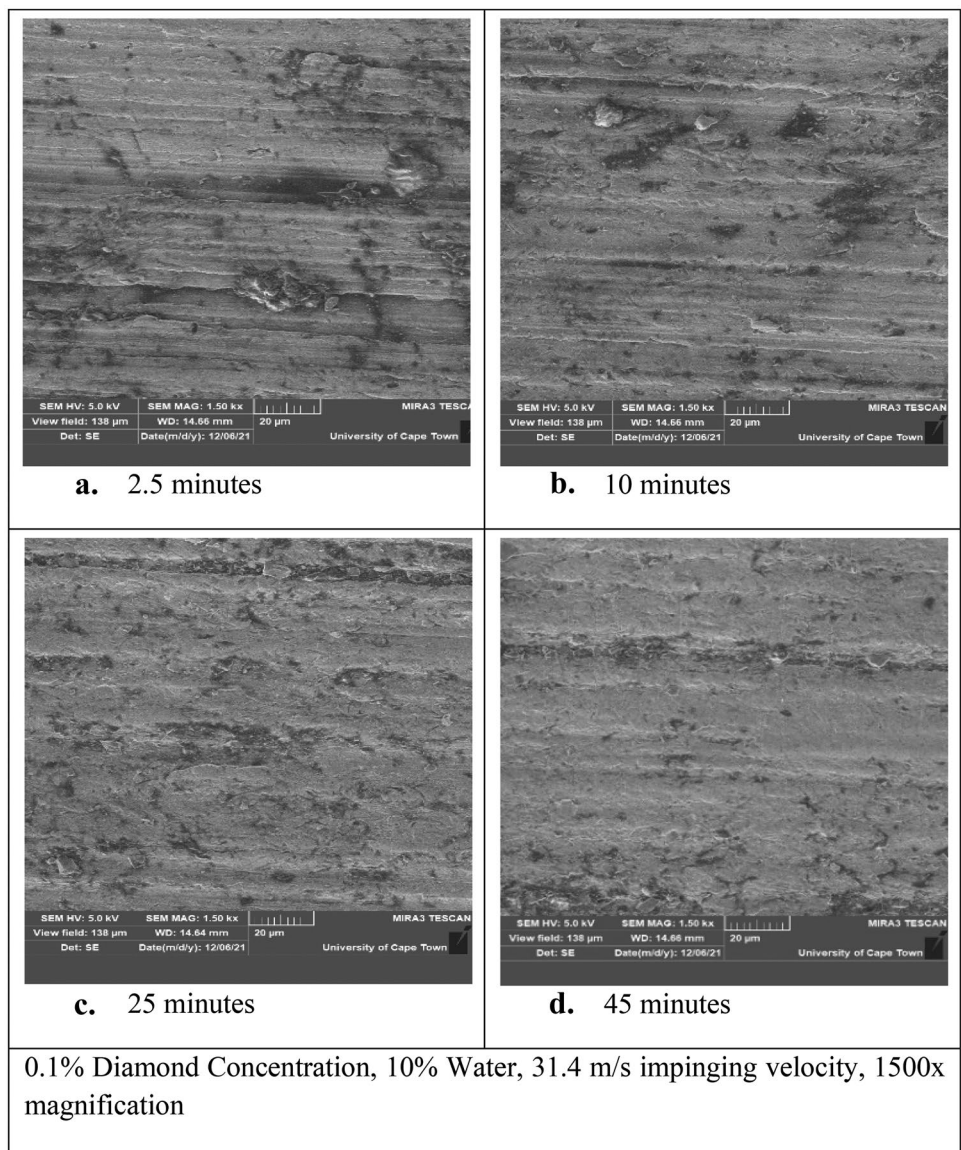
equilibrium is reached (therefore higher displacements). This damping ratio agrees well with contact time results and force results as higher hydrations show more underdamped results and this implies longer contact times as well as lower contact forces. Damping ratios closer to critical imply less deformation (which was again found in the previous section) and less contact time. This also aligns with the previous section which shows that higher contact times are associated with higher hydration levels and lower kinetic energies.

Damping coefficient is relative to the system as mass plays a large role in its determination and it can vary from case to case, but the results (Fig. 28) show that damping coefficient has a similar trend to damping ratio (with more dramatic decreases as hydration is increased), which helps to affirm the previously discussed results.

An important result of the vibrational analysis (which serves as an input for a large array of contact mechan-

ics relations) is that of contact deformation. This was calculated in the previous section and plotted over time; however, in contact mechanics, the deformation of interest is that of maximum deformation (which is when the abrasive will be applying maximum force upon the workpiece). Figure 29 shows that deformation increases logarithmically (with a sharp initial gradient) as kinetic energy is increased. Dry contact deformation does not bare much difference to 10% hydration contact deformation; however, 30% and 50% hydration show great increases in deformation (approximately $1.7 \times$ and $2.3 \times$ increases respectively). This is due to the great reduction in stiffness as well as the lower damping ratios. Again, the results match those of Fukumoto et al. [13]. Higher deformation is incurred by higher contact times (meaning lower contact forces). This agrees with the experimental results acquired (lower forces at higher hydration

Fig. 22 1500X SEM images for 10% hydration and 31.4 m/s impinging velocity. **a** 2.5 min, **b** 10 min, **c** 25 min, **d** 45 min



levels) as well as the better texture and quality results shown in the SEM images.

Finally, and of interest to the material removal mechanism, the results of contact stress are shown (Fig. 30). The results are displayed as a unitless function of dry contact stress to adequately show the effect of hydration and kinetic energy on contact stress. Unitless presentation is also selected because the micro and nano contact stresses (between diamond/SiC and Ti-6Al-4V asperities), which cause the most abrasive removal by ductile polishing, cannot be separated in this model (which accounts for the viscoelastic contact of gelatin, while SiC and diamond barely contribute to the overall system stiffness). In agreement to

the displacement results, the contact stress drops minorly when using 10% wet abrasives and then becomes much smaller at 30% and 50% (approximately 25% and 18% of the dry contact, respectively). Kinetic energy plays much less of a role in the determination of contact stresses at higher hydrations and this shows that greater damping is occurring at higher levels of hydration.

Table 7 shows a comparison of results for the experimental measurements and theoretical model as well as a comparison to the previous research. Presented results and gathered research (where comparison is possible) trends tend to agree with each other and thus model validation is present.

Fig. 23 1500X SEM images for 30% hydration and 15 m/s impinging velocity. **a** 60 s, **b** 180 s, **c** 300 s

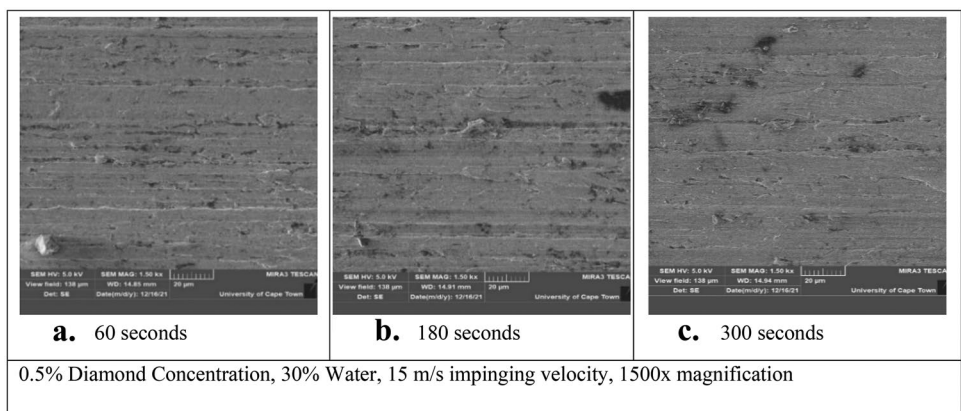


Fig. 24 1500X images for 30% hydration and 6.28 m/s impinging velocity. **a** 60 s, **b** 180 s, **c** 300 s

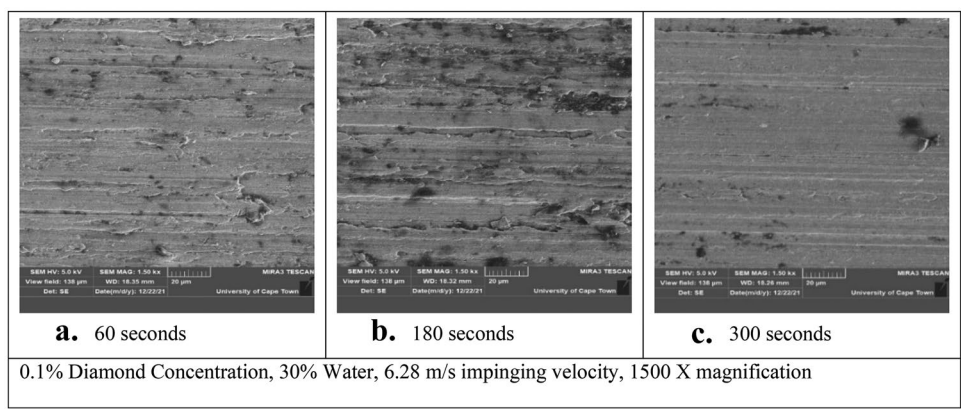


Fig. 25 500X images for 5 min polishing and 31.4 m/s impinging velocity. **a** 10% hydration, **b** 50% hydration

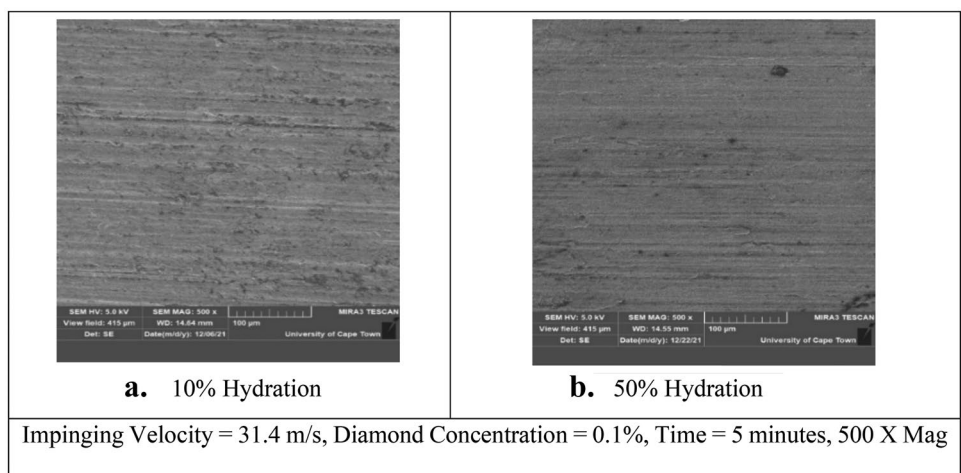


Fig. 26 1500X SEM images for 5 min polishing and 31.4 m/s impinging velocity. **a** 10% hydration, **b** 50% hydration

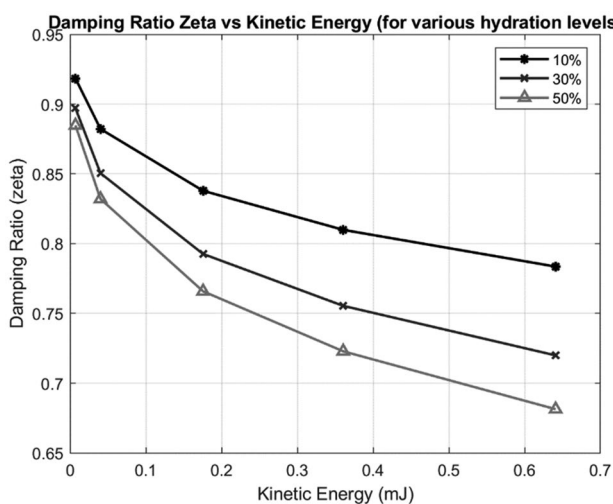
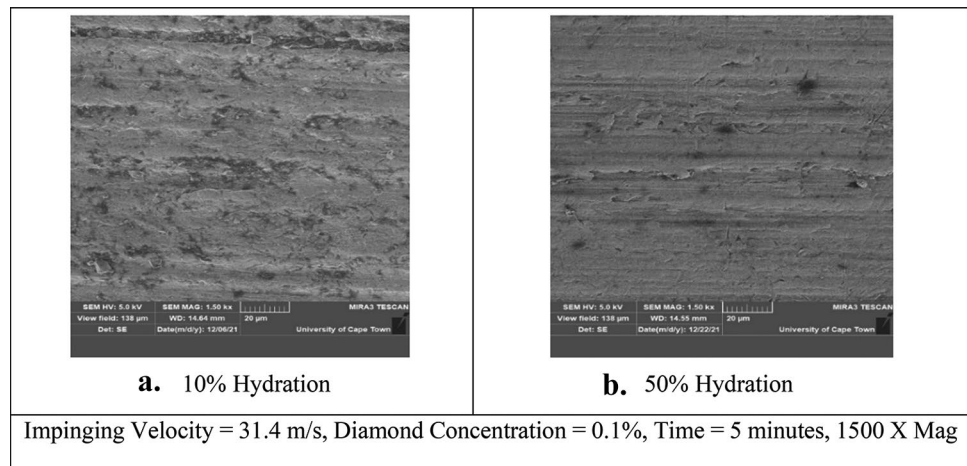


Fig. 27 Damping ratio results

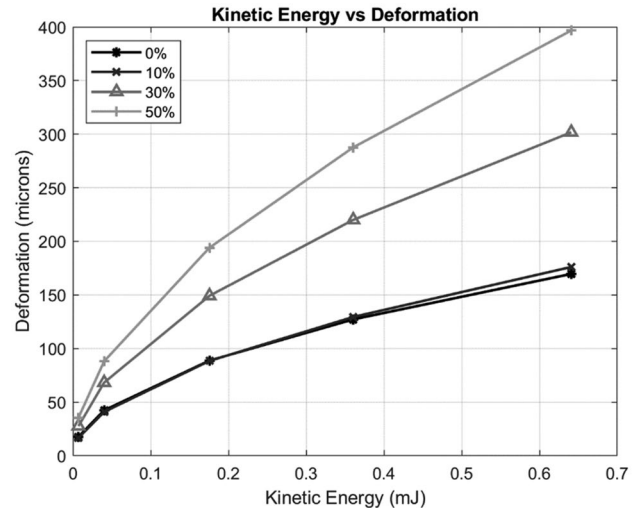


Fig. 29 Deformation as a function of kinetic energy (for various hydration levels)

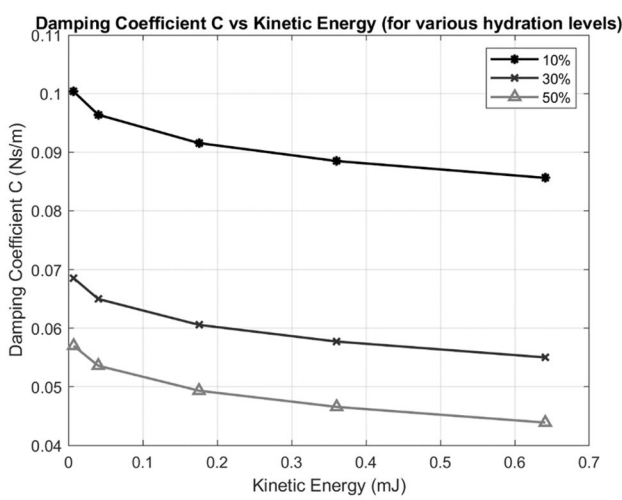


Fig. 28 Damping coefficient results

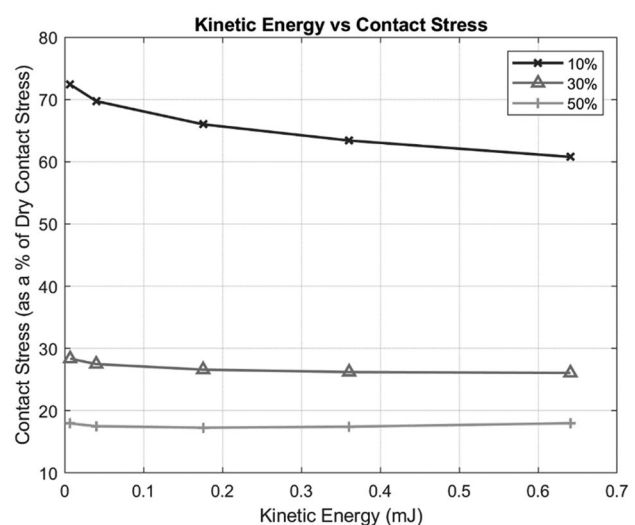


Fig. 30 Contact stress (as a percentage of dry contact stress) as a function of kinetic energy (for various hydration levels)

Table 7 Summary of results

	Experimental measurements	Theoretical model	Past research
Impact force	Higher hydration implies less impact force	Agree with experimental	Agree with experimental and theoretical [2, 19]
Contact time	Not presented in this paper	Greater contact times at higher hydrations	Agree with theoretical [13]
Surface roughness	Lower convergence over longer time at higher hydrations	Not presented in this paper	Agree with experimental [1, 2, 18]
Damping ratio		Less at higher hydrations (further away from critical)	Implied less by lower contact stress (agrees with theoretical) [2, 13]
Deformation/contact area	Implied greater at higher hydration due to lower forces	Greater at higher hydrations	Agree with theoretical [13]
Contact stress	Implied less at high hydrations due to lower forces	Less at higher hydrations	Agree with theoretical [2, 13]

6 Conclusion

This paper has presented a viscoelastic model for the blast polishing of Ti-6Al-4V surfaces, with experimental results presented along with an adapted empirical-analytical force model (based on Hertzian contact mechanics and the notion of critical values) to account for varying kinetic energies of impact and hydration levels of abrasive. Critical values are based on experimentally gathered results where the change from elastic to plastic deformation in contact occurs. The use of typical Hertzian contact parameters such as contact stress then allows for the determination of force values.

The results of the force model agree with experimental research presented as well as with experiments done by other authors on blast polishing (who had notably used momentum equations to gather force data). Impact forces were found to decrease dramatically with increases in hydration levels (1.3 N at 0% hydration to 0.35 N at 50% hydration, for the highest levels of kinetic energies), while increasing with kinetic energy. Contact times were inferred using conservation of momentum and were found to increase significantly as hydration levels are increased (from 18 to 78 μ s for the highest kinetic energies at 0% and 50% hydrations, respectively).

Damping ratios were found to be close to critical at low values of kinetic energy while they rapidly became more underdamped as kinetic energy was increased. Higher values of hydration also result in lower values of damping ratio and the same trend was detected in the damping coefficient.

Maximum contact deformation was found to be similar for dry contact and 10% wetness, before dramatically increasing when wetness was increased to 30% and 50%. This analogy again agrees with that of experimental studies and the force model. Contact stress decreases significantly as hydration levels are increased (50% hydrated media impacting a workpiece

provides 325% less contact stress than 10% hydrated media). This proves that higher hydration aids in allowing a polishing process to occur at higher velocities, while imparting less damage to the surface of the workpiece.

When concerning choice of polishing conditions/parameters, the authors are in agreement with previous researchers when stipulating that a 45° polishing angle (to balance removal and biting force), a low standoff distance of 20 mm (to ensure minimal loss of media impinging velocity and angle) and an output nozzle area smaller than the workpiece area (to ensure media is directed properly and to achieve a maximum media output rate) aid in achieving optimal polishing conditions. The authors also recommend (due to the results garnered and the agreement of results with other researchers) that a high hydration (of 30 to 50%), a high impinging velocity (31.4 to 59.5 m/s), and a polishing time of 20 to 40 min be used to achieve optimal polishing conditions. These results are based on an additive manufactured (SLM) Ti-6Al-4V component but can easily be extended and modified to other materials (particularly due to the nature that Ti-6Al-4V is a difficult to machine component and thus presents an extreme polishing case).

Author contribution Quintin de Jongh: writing original draft, investigation, conceptualization, methodology, machine/process design and development, experimentation, model development, and validation. Ramesh Kuppuswamy: supervision, project administration, resources, validation and investigation, and support writing. Matthew Titus: conceptualization, machine/process design and development, and investigation.

Funding This project was supported by fund NRF GRANT: INCENTIVE FUNDING FOR RATED RESEARCHERS (IPRR) –South Africa through Reference: RA191118492767 and Grant No: 136118. The views expressed and the conclusions drawn in this paper are those of the authors and cannot necessarily be attributed to the references.

Availability of data and materials The authors confirm that the data supporting the findings of this study are available within the article.

Declarations

Ethics approval The author(s) confirm that the paper has not been published previously in any form or language that it is not under consideration for publication elsewhere and does not contain material which has been published previously. The results are presented clearly, honestly, and without fabrication, falsification, or inappropriate data manipulation.

Consent to participate Not applicable.

Consent for publication Not applicable.

Competing interests The authors declare no competing interests.

References

- Kuppuswamy R, Ozbayraktar S, Saridikmen H (2012) Aero-lap polishing of poly crystalline diamond inserts using Multicon media. *J Manuf Process* 14(2):167–173. <https://doi.org/10.1016/j.jmapro.2011.12.003>
- Nizar M (2016) Influence of surface modification by blast polishing method on the cutting performance of carbide tool. Toyohashi University of Technology, Doctoral Dissertation
- Nishimura Y, Endob M, Yanaseb K, Ikeda Y, Miyakawa S, Miyamoto N (2016) High cycle fatigue strength of spring steel with small scratches. Proceedings of First Structural Integrity Conference and Exhibition, Bangalore
- Huang H, Gong Z, Chen X, Zhou L (2002) Robotic grinding and polishing for turbine-vane overhaul. *J Mater Process Technol* 127(2):140–145. [https://doi.org/10.1016/S0924-0136\(02\)00114-0](https://doi.org/10.1016/S0924-0136(02)00114-0)
- Kitajima K, Yamamoto A (2010) Latest trends in deburring technology. *Int J Autom Technol* 4(1):4–8. <https://doi.org/10.20965/ijat.2010.p0004>
- de Jongh Q, Kuppuswamy R, Titus M (2022) A force controlled polishing process design, analysis and simulation targeted at selective laser melted Ti6Al4V aero-engine components. International Conference on Competitive Manufacturing, Stellenbosch
- Wang M, Qin P, Zan T, Gao X, Han B, Zhang Y (2021) Improving optimal chatter control of slender cutting tool through more accurate tool mass damper modeling. *J Sound Vib* 513:1–16. <https://doi.org/10.1016/j.jsv.2021.116393>
- Naghieh G, Rahnejat H, Jin Z (1997) Contact mechanics of viscoelastic layered surface. *Transactions on Engineering Sciences* 14:59–68. <https://doi.org/10.2495/CON970071>
- Assie A, Eltaher M, Mahmoud F (2010) Modeling of viscoelastic contact-impact problems. *Appl Math Model* 34:2336–2352. <https://doi.org/10.1016/j.apm.2009.11.001>
- Hunek I (1993) On a penalty formulation for contact-impact problems. *Comput Struct* 48(2):193–203. <https://doi.org/10.1016/0045-7949%2893%2990412-7>
- Fahmy M (2000) A computational model for elastic-plastic dynamic contact, Ph.D dissertation. Zagazig University, Doctoral Dissertation
- Lopez-Guerra EA, Solares SD (2014) Modelling viscoelasticity through spring-dashpot models in intermittent-contact atomic force microscopy. *Beilstein J Nanotechnol* 5:2149–2163. <https://doi.org/10.3762/bjnano.5.224>
- Fukumoto M, Takai K, Nizar M, Arimatsu N, Uemura M (2016) Study on polishing mechanism of cemented carbide by blast polishing. 3rd Report: influence of water content in polishing media on polishing mechanism. *J Abras Process Soc* 60(5):261–266. <https://doi.org/10.11420/jsat.60.261>
- Bulicek M, Malek J (2012) On Kelvin-Voigt model and its generalizations. *Evol Equ Control Theory* 1(1):17–42. <https://doi.org/10.3934/eect.2012.1.17>
- Roberts J, Jones R, Rothberg S (2001) Measurement of contact time in short duration sports ball impacts: an experimental method and correlation with the perceptions of elite golfers. *Sports Eng* 4:191–203. <https://doi.org/10.1046/j.1460-2687.2001.00084.x>
- Hocknell A (1998) Computational and experimental analysis of elastic deformation in impact, PhD thesis. Loughborough University, Doctoral Dissertation
- Goldsmith W (1960) Impact: the theory and physical behaviour of colliding solids, Edward Arnold (Publishers) Ltd., London
- Draganova D, Izarkova G, Guzanova A, Brezinova J (2018) General regression model for predicting surface topography after abrasive blasting. *Metals* 8(11):1–21. <https://doi.org/10.3390/met8110938>
- Takai K, Nizar M, Uemura M, Fukumoto M (2014) Study on the polishing mechanism of cemented carbide using blast polishing process. 2nd report: effect of kinetic energy and injection angle on surface condition of cemented carbide. *J Jpn Soc Abras Technol* 58(6):386–291. <https://doi.org/10.11420/jsat.58.386>
- Okamoto (Thai) Co., Ltd. (2020) Mirror finishing technology for improvement of mold releasability. MReport. <https://www.mreport.co.th/en/experts/technology/015-Mirror-Finishing-Technology-for-Mold-Releasability-Okamoto-Aero-Lap>. Accessed 24 Nov 2021
- Takai K, Nizar M, Uemura M, Fukumoto M (2013) Polishing mechanism of cemented carbide using blast polishing process. 1st report: effects of injection speed and polishing time on surface roughness. *J Jpn Soc Abras Technol* 57(4):253–258. <https://doi.org/10.11420/jsat.57.253>
- Jackson R, Ghaednia H, Lee H, Rostami A (2013) Contact mechanics, tribology for scientists and engineers. Springer Science+Business Media, New York

Publisher's note Springer Nature remains neutral with regard to jurisdictional claims in published maps and institutional affiliations.

Springer Nature or its licensor holds exclusive rights to this article under a publishing agreement with the author(s) or other rightsholder(s); author self-archiving of the accepted manuscript version of this article is solely governed by the terms of such publishing agreement and applicable law.